Composite repair for aeronautical structures

Francis Collombet[a], Yves Davila[a], Sergio Avila[b], Alexander Morales[b], Laurent Crouzeix[a], Yves-Henri Grunevald[c], H. Hernandez[b], Bernard Douchin[a], Nathalie Rocher[a], François Cénac[d]

a. Université de Toulouse, UPS, INSA, Mines d'Albi, ISAE, ICA (Institut Clément Ader). Espace Clément Ader, 3 rue Caroline Aigle, 31400 Toulouse. France.
francis.collombet@iut-tlse3.fr, yves.davila@iut-tlse3.fr, laurent.crouzeix@iut-tlse3.fr, bernard.douchin@iut-tlse3.fr, nathalie.gleizes@iut-tlse3.fr
b. Instituto Politecnico Nacional, ESIME Ticoman. Av. Ticoman N° 600, 07340 Ciudad de Mexico. Mexico.
saavilah@ipn.mx, almoralesg@ipn.mx, hihernandezm@ipn.mx
c. Composites, Expertise & Solutions. 131 Traverse de La Penne aux Camoins, 13821 La Penne-Sur-Huveaune. France.
yh.grunevald@composites-expertise-solutions.com
d. Bayab Industries. 10 allée de Longueterre, 31850 Montrabé. France.
f.cenac@bayab.fr

Résumé:

On se propose de dérouler l'ensemble des étapes de la réparation d'une structure composite primaire aéronautique et de présenter les outils numériques facilitant l'analyse du comportement mécanique de la zone réparée. Afin de valoriser différents aspects de l'approche présentée, on choisit une structure parent simple formée de 16 plis d'UD Hexply® M21/35%/268/T700GC et présentant une séquence d'empilement de type $[+45/-45/-45/+45/+45/-45/-45/+45]_s$*. La réparation est dite en escalier par recouvrement des plis successifs et 3 valeurs de longueur de recouvrement (6, 8 et 13 mm) sont étudiées. Après usinage par jet d'eau abrasif et réalisation d'un patch de réparation, les plaques parent sont découpées en éprouvettes sollicitées en traction simple dans une direction de chargement qui est à 45° par rapport à celle des fibres. On montre que le maillon faible de la réponse mécanique correspond à la zone monolithique non réparée et que le niveau des contraintes de cisaillement pour les trois choix de longueurs de recouvrement est bien en dessous de la valeur limite du film adhésif utilisé. Cette étude souligne la valeur ajoutée d'un brevet (co détenu par l'ICA, Bayab Industries et CES) qui suscite l'intérêt d'Airbus afin de réduire l'emprise des patchs de réparation. Il permettra ainsi à nombre de situations (en fabrication ou en service) de pouvoir être réparées par simple collage d'un patch sans adjonction de doubleurs rivetés.*

Abstract:

This paper proposed to carry out all stages of primary aeronautical composite structure repair as well as numerical tools facilitating the cross-over analysis of the repaired area mechanical behaviour. In order to promote different aspects of the approach, a simple parent structure consisting of 16 plies of UD Hexply® M21/35%/268/T700GC is chosen with a stacking sequence of $[+45/-45/-45/+45/+45/-45/-45/+45]_s$*. The repair is called step lap by overlapping successive plies and 3 values of overlapping length (6, 8 and 13 mm) are investigated. After abrasive water jet machining and repair patch manufacturing, specimens are cut to be tested in a uniaxial tensile configuration with a loading direction*

shifted 45° compared to fiber direction. It is shown that the weak link in the mechanical response is the unrepaired monolithic area and the level of shear stress in the adhesive film, for these three overlapping values, is below the limit value. This study highlights the added value of a patent (jointly owned by ICA, Bayab Industries and CES) having Airbus' interest for reducing repair patch dimensions. It will allow many situations (in manufacturing or in service) to be repaired by patch adhesive bonding without additional riveted doublers.

Keywords: Composite repair, Abrasive Water Jet machining, finite elements models

1 Introduction

The purpose of this paper is to present the scientific and technical issues related to the repair of aeronautical structures, made of multilayer monolithic long fibre composites, for which there is an increased need due to the entry into service of hundreds of B787 or A350 aircrafts per year. In the repair process, one of the issues is to limit the influence of this area of removal of material and reducing the prohibitive time of immobilization of the aircraft (which costs 100 to 200 kUS dollars by day). To illustrate our purpose, the studied plate consists of 16 plies of UD Hexply® M21/35%/268/T700GC prepreg and presents a stacking sequence $[+45/-45/-45/+45/+45/-45/-45/+45]_s$. The first stage of this study corresponds to a machining phase using an abrasive water jet technique. This phase is performed with the mobile machine REPLY.5, designed by the innovative small company Bayab Industries, which is the only machine certified by Airbus to repair primary structures on the A350 [1]. The patch polymerization is done using the portable hot bonder Aeroform AHB-380. Different overlap lengths (6, 8 and 13 mm) are considered to surround the overlapping value recommended in aeronautics. Indeed, the overlapping distance is expressed as a ratio of the ply thickness, and, in aeronautics, this ratio is usually 30 (which is roughly the ratio between 8 mm overlap length and 0.26 mm ply thickness), whatever the fibre orientation versus the main loading direction. Test coupons cut from mother plates with these three overlap ratios, 20, 30 and 50 respectively, are used to perform uniaxial tests in a 45° loading direction from the one of the long fibre reinforcements. This choice of loading and material orientation is a manner to study if a nominal overlap length is strictly necessary in the direction of the UD fibres. It leads to a contribution of the interest of the joint patent held by the Clement Ader Institute, the SME Composites Expertise & Solutions and the TPE Bayab Industries [2]. This patent allows the description and modelling of a minimum volume of material to be removed while ensuring a nominal transfer of efficient stress flow between the parent composite part and the repair patch. Complementary to the experimental investigation, a finite element study is performed in parallel. The repair zone is modelled through an innovative multi-scale method [3] in which the composite substrates are modelled through shell elements and the adhesive joint consists of volume elements. The aim is to avoid the use of overly heavy finite element calculations, which penalizes the design of large repaired structures, making cross-test calculations very time-consuming. The numerical model shows that the overlap length is not the weak link of these coupons behaviour since the limit of damage initiation is reached in the non-repair zone of the specimens and not in the repair patch zone. These numerical results correlate the experimental observations.

2 Abrasive water jet machining process

The first stage of this study corresponds to the fabrication and machining process of a monolithic carbon-epoxy composite plate. For this study a 16 plies composite plate of [+45°/-45°/-45°/+45°/+45°/-45°/-45°/+45°/+45°/-45°/-45°/+45°/+45°/-45°/-45°/+45°] i.e. $[((+45°/-45°)_s)_s]_s$ is made. The latter is made from a UD Hexply® M21/35%/268/T700GC prepreg, cured in autoclave at 180 °C. Afterwards

the plate is cured and then machined. Three step ratios (step length over ply thickness) are studied, 20, 30 and 50, which roughly correspond to overlap lengths of 6 mm, 8 mm and 13 mm respectively.

The machining is done through the abrasive water jet (AWJ) removal technique. The AWJ machining is performed by a mobile machine (REPLY.5) designed by the French innovative small company Bayab Industries. This equipment is the only mobile machine certified by Airbus for the material removal of primary composite structures of the A350 [1].

The AWJ technique allows an offset machining "layer by layer", unlike the mechanic tools used by the conventional techniques [2], as a stepping, in order to carry out the repair via a patch covering plies.

The REPLY.5 AWJ machine consists of three principal elements, the control unit which contains the pump and the control system (cf. Figure 1a), the abrasive water jet equipment and the control panel to operate the machine (cf. Figure 1b).

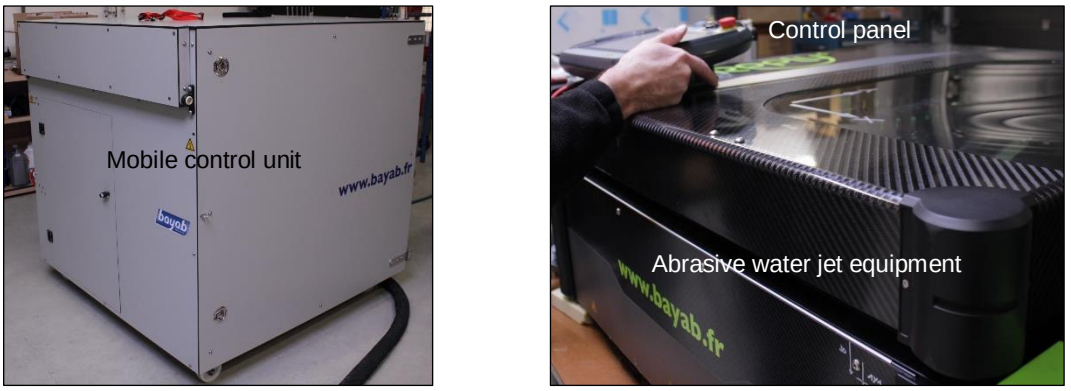

a) b)

Figure 1. Bayab Industries abrasive water jet machine REPLY.5 with a) control unit and b) abrasive water jet equipment and control panel.

After fixing the composite plate onto the workbench, the AWJ machine is placed on top of it and is maintained in position with suction cups (cf. Figure 2a). In an industrial situation, this suction system allows the positioning of the machine onto a composite fuselage. The machine is then levelled to ensure perpendicularity of the abrasive water jet nozzle with the surface of the plate (cf. Figure 2b). The waste generated during the machining process, composed by composite dust, abrasive particles and water, is removed by an aspirator system.

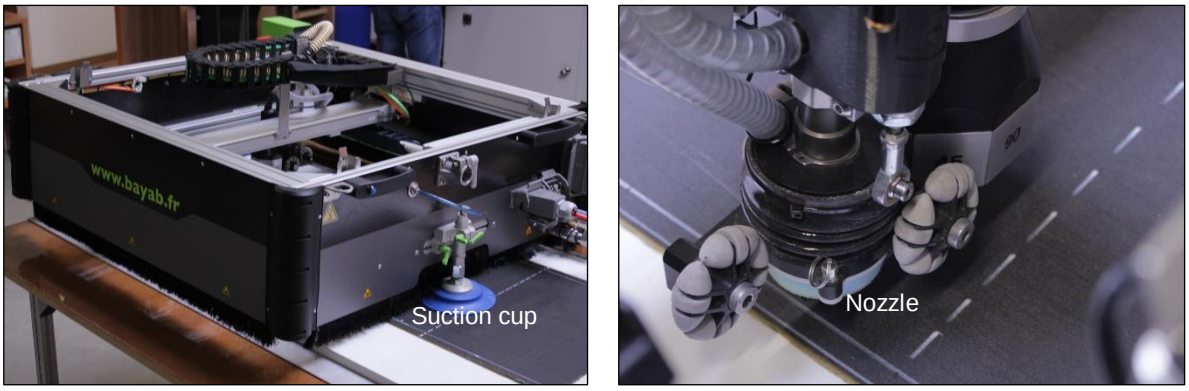

a) b)

Figure 2. Bayab Industries abrasive water jet machine Reply.5 with a) levelled machine and b) nozzle.

The machine is aligned by a laser level to the marked along the x- and y- main directions of the composite plate (cf. Figure 3).

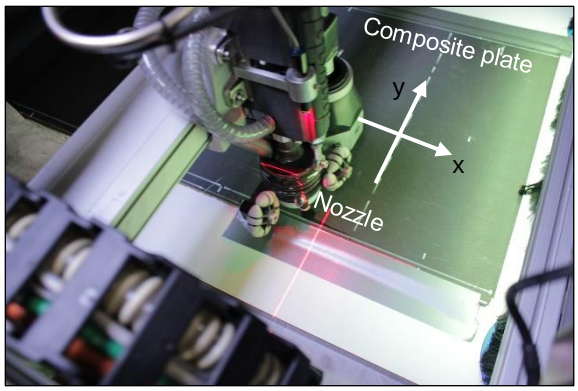

Figure 3. Alignment process of the nozzle over the x- and y- main directions of the composite plate.

After aligning the machine, the layer of composite material corresponding to the first step (here ply #16) is removed. As an illustration, the first machined step for the step lap ratio of 20 is presented in Figure 4. For the other step lap ratios of 30 and 50, the same procedure is applied. The cut trajectory and cut parameters (water jet pressure, and nozzle feed rate) are programmed into the machine. These parameters are Intellectual Property of Airbus and Bayab Industries and have not been disclosed.

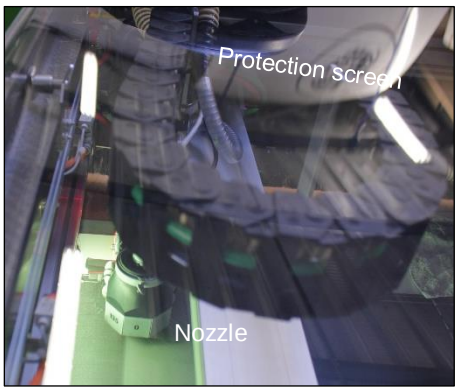

Figure 4. View through the protection screen of the machine during the machining of the step 1 for the step lap ratio of 1:20.

Once the machining process in one ply is finished, a verification is done by means of image analysis using the camera installed on the AWJ machine and a lighting of the machined zone through a set of four low-angled lights aiming in the four possible orientations of the reinforcement, 0°,90°, +45° and -45° (cf. Figure 5a). To verify the fibre direction of the below ply, the camera takes four different images using each lighting angle. Indeed, the lightning emitted by the low-angled light is diffracted differently depending on the angle with respect to the long fibre orientation. The control unit compares the recorded images pixel-by-pixel. For accurate information, a selection of images from the screen of the control panel (cf. Figure 5b) shows an estimation of the matrix ratio in an interface between two plies and is evaluated to ensure that just one ply was removed. This is an alternative to direct measurement of the cut depth.

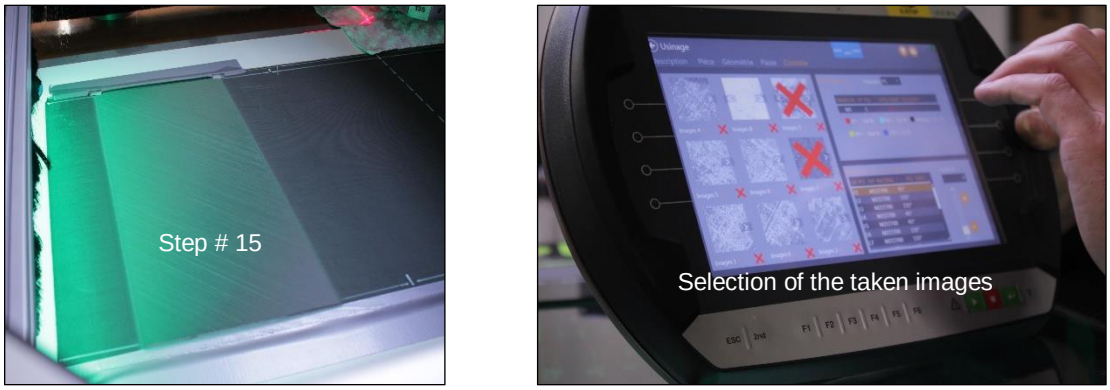

a) b)

Figure 5. Verification process of the machining surface with a) overlap lap analysed by image analysis and b) visualization and selection of the taken images on the control panel to estimate whether or not the interface is reached.

Afterward, the process or nozzle alignment, machining and verification are repeated. As illustration, the resulting step lap profile (ratio of 20) is shown in Figure 6.

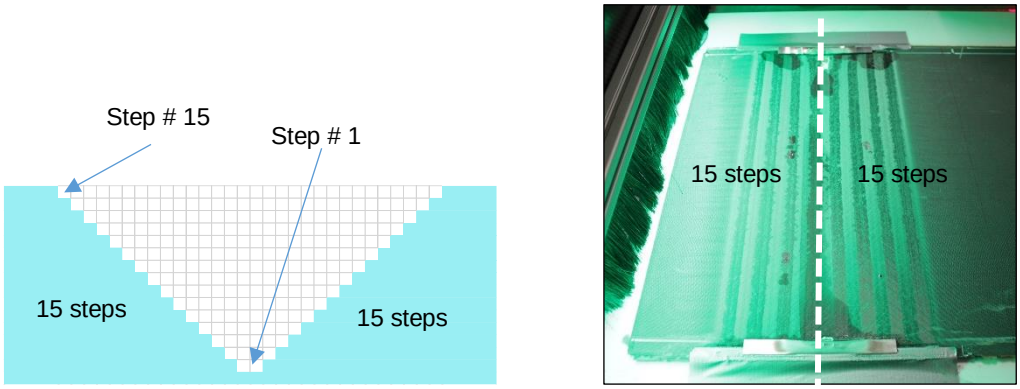

a) b)

Figure 6. Machining of the 15 steps with a) scheme of machined profile (not to scale) and b) view of the finished machined step lap for the overlap lap ratio of 20.

3. Repair process

When the machining process is complete, the composite plates are cut in halves in order to create the possibility of repairing two sets of plates for each overlap ratio (cf. Figure 6). We label Plate 13 (for step length of 13 mm) the parent plate corresponding to a step ratio of 50 which is the one shown on Figure 7 and hereafter as an illustration in this paper. The repair material of the reconstituted zone is the same one as the parent plate, Hexply® M21/35%/268/T700GC. The curing process, however, will be performed by a portable hot bonder machine under only vacuum instead of being placed into an autoclave. This situation is different to the Airbus repair because the repair material for the patch is different to the parent material which is typically cured at 120°C.

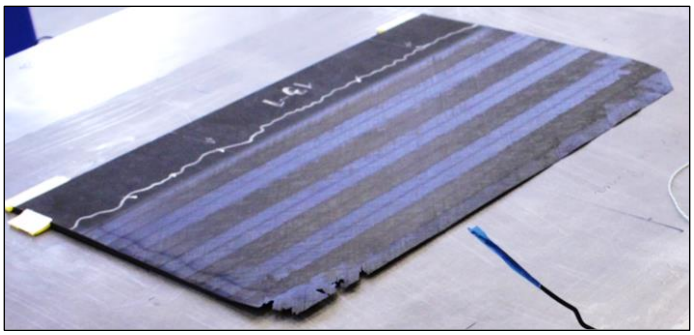

Figure 7. Parent composite plate noted Plate 13 (overlap length of 13 mm) shown before the repair patch installation.

An adhesive film of Hexcel Composites Hexbond® is placed between the repair plies and the parent plate. This film is cured at 175°C, to be compatible with the cure cycle of M21 resin of the repair plies.

The surface of the repair is degreased and cleaned using alcohol and/or acetone. The repair procedure is composed of different phases. First, the adhesive film of Hexbond® is placed in the repair area (cf. Figure 8a). Then, the repair plies are stacked using a guide drawn on the surface of the tooling for adequate ply placement, for the first ply (cf. Figure 8b) to the sixteenth repair ply (cf. Figure 8c).

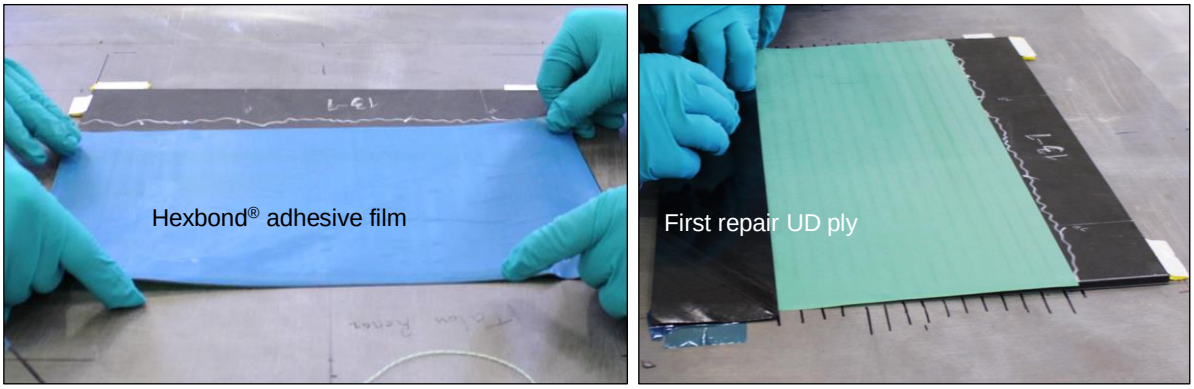

a) **b)**

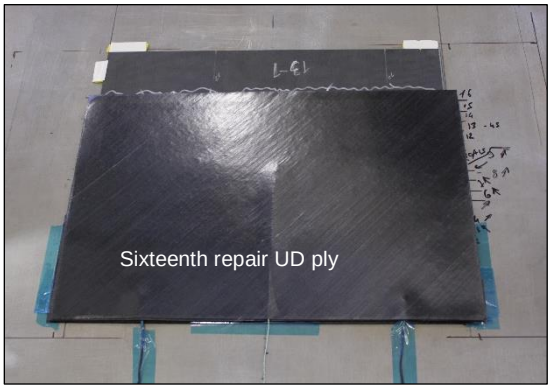

c)

Figure 8. Repair patch installation with a) installation of the Hexbond® adhesive film with its protective plastic film, b) placement of the first repair ply and c) after the placement of the sixteenth repair ply.

Once all the repair plies are laid up, the vacuum bag is installed. The sequence of vacuum bag materials is done in accordance with Airbus Structural Repair Manual indications for structural composite repair (cf. Figure 9).

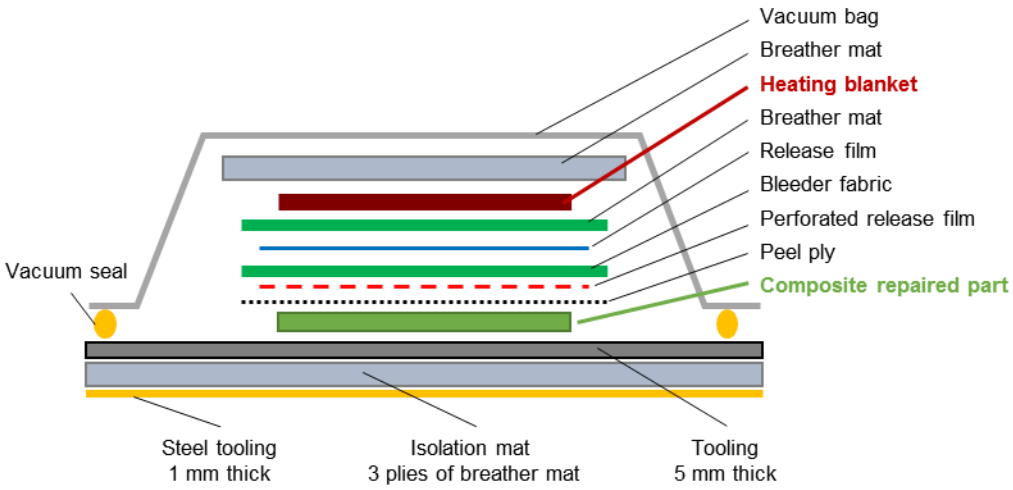

Figure 9. Scheme of the vacuum bag products (not to scale) for the composite patch curing by heating blanket (according to SRM A350 chapter 51.77.11, [1]).

Once the vacuum bag is placed and sealed, a vacuum test is performed. The vacuum is applied using the external vacuum pump (cf. Figure 10).

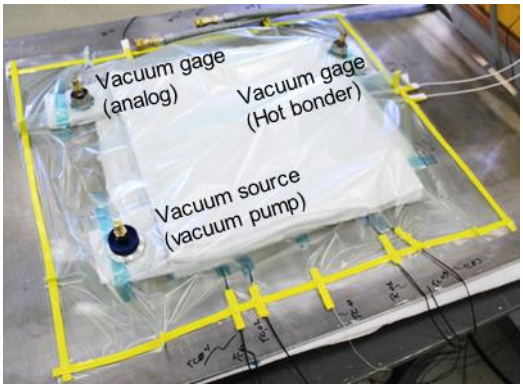

Figure 10. Overview of the vacuum bag products and the outgresses of the different thermocouples.

The temperature cycle is programed into the hot bonder (cf. Figure 11). The M21 resin cures at 180 °C for 2 hours. An intermediate dwell at 100 °C during 30 min is used in order to homogenise the temperature in the unconsolidated patch prepreg and to promote the movement of resin and removal of entrapped air causing porosities in the material. The temperature ramps are set at 3 °C min^{-1}. The vacuum is applied with an external portative vacuum pomp (cf. Figure 11).

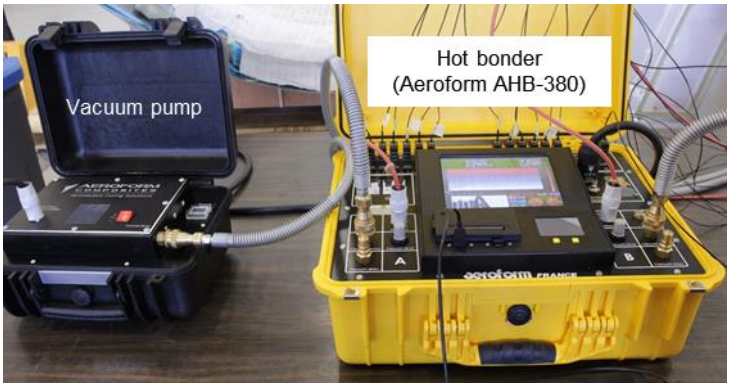

Figure 11. View of the portable hot bonder Aeroform AHB-380 (right) and the portable vacuum pomp (left).

When the curing cycle is complete, the part is demoulded. The resulting piece is shown in Figure 12. Finally, coupons for tensile test are cut from the repaired mother plate using an abrasive water jet machine. The central zone is only considered to eliminate the damage in the boundary of the parent plate.

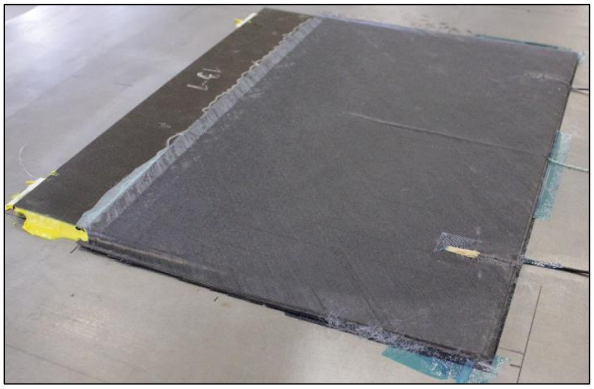

Figure 12. View of finished repair on plate 13 after curing (overlap length of 13 mm).

4. Finite Element models and test results

A light finite element (FE) modelling strategy is used [3]. This strategy uses shell elements for the composite laminate and volume elements for the adhesive joint (cf. Figure 13). The mesh of the composite parent zone is modelled using shell element of 0.44 x 0.44 mm dimensions. One volume element of 0.1 mm thick with the same width and length that the composite shell elements is used to model the adhesive film with a thickness to length ratio of 1:4. To assure a continuous transfer of stresses and nodal displacements, each segment of the step repair is linked to the previous one using rigid beam elements. In our applications, there was no adhesive rupture but only cohesive one if any. No use of cohesive element is required. This light modelling strategy allows the reduction in computation time and facilitates the experiment/calculation comparisons. The initial implementation of this methodology was programmed in Samcef code [3], and it was successfully applied in Abaqus code. Details of the number of elements and the degrees of freedom for each 6, 8 and 13 mm overlapping length models are given in Table 1.

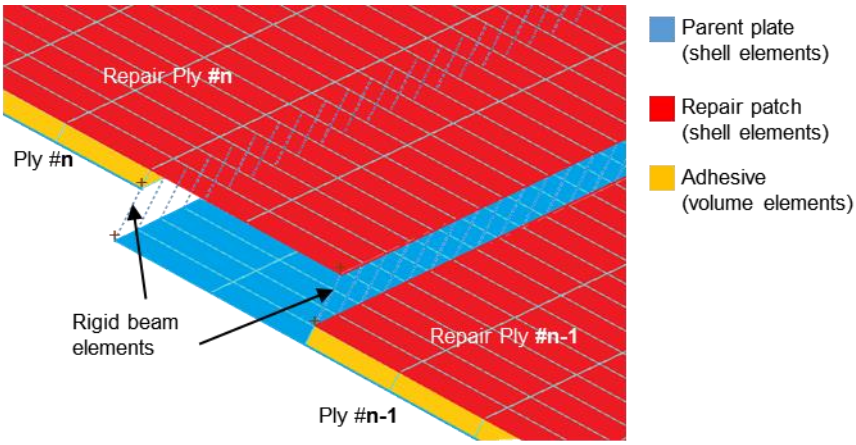

Figure 13. Mesh detail between two consecutive steps (ply #n and #n-1).

Table 1. Definition of the three meshes.

Step size (mm)	6	8	13
Number of Finite Elements	48 000	58 000	86 000
DoF (Abaqus variables)	309 000	367 000	542 000

The shape of the tensile repaired coupon is shown in Figure 14. The repaired coupon is 22 mm wide in the gauge zone, corresponding to the overlap zone. Its end tabs are 30 mm wide in order to avoid a possible material failure at the machine clamps. The zone having 20 mm length approximately located between the overlap and the tab is considered as representative of a non-repaired area. This zone corresponding to the non-repaired zone of the parent zone has the original mother plate of 16 plies, while the reconstituted material in the patch area has one extra ply (repair ply #0) with the same orientation as the repair ply #1. This zone has a stacking sequence with 17 plies in total in accordance with composite repair implementation (cf. Figure 15). Figure 15 uses white arrows to show the loading flow transfer principle from the parent plies to the repair plies.

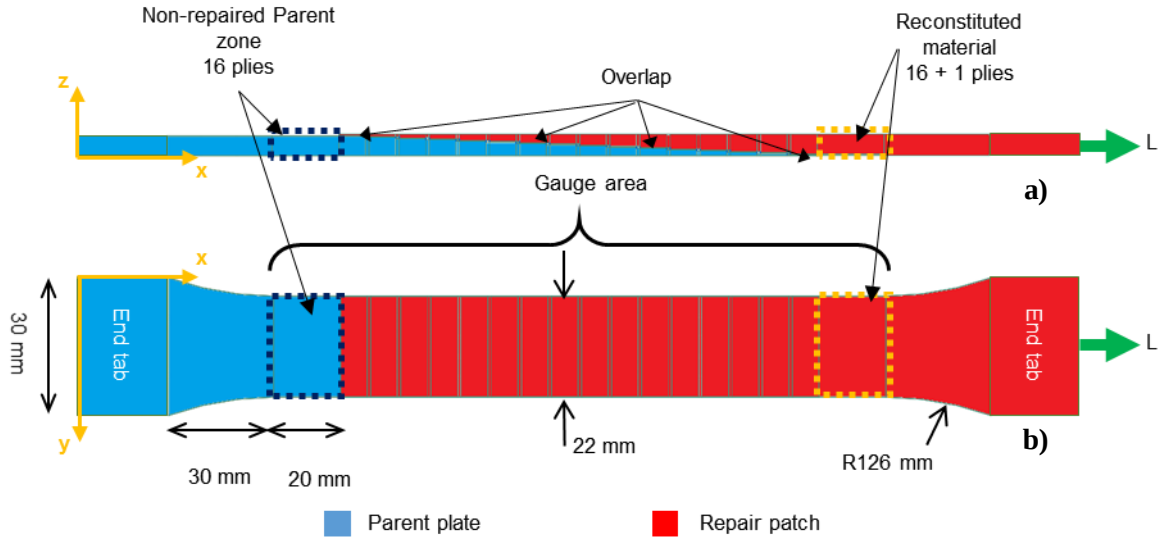

Figure 14. 3D representation of the FE model (shell thicknesses rendered at their given values) with a) side view (XZ plane) and b) top view (XY plane).

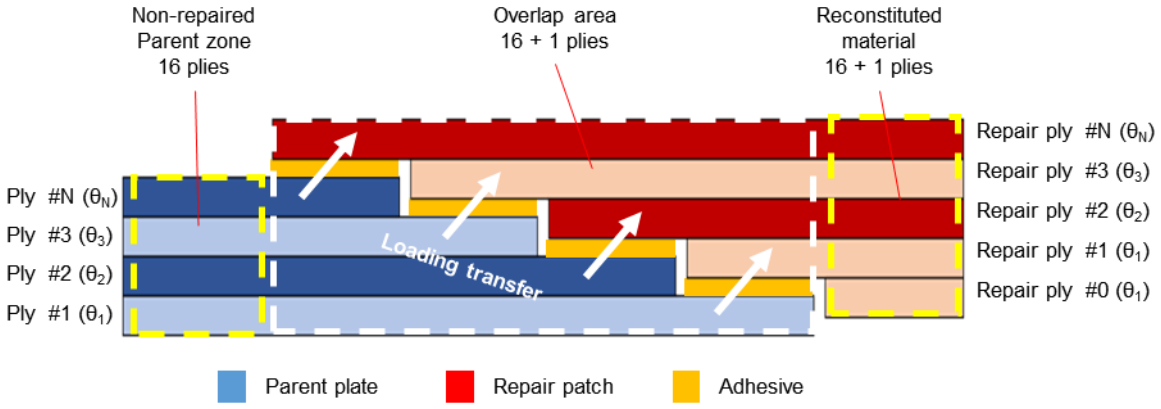

Figure 15. Scheme of composite repair considerations overlapping (not to scale).

In this study, we are not concerned by the ultimate tensile strength of the coupon, according to the aeronautic specifications of work for which no damage is allowed. The behaviour of the ±45° tensile test is matrix dominated, and having the fibres oriented at an angle different from the loading direction, the resulting axial stress – strain curve begins not linear because of the damage initiation in the matrix. We are interested to study the performance of repair while the 16-ply monolithic non-repaired zone of the material is within its linear regime just before the damage initiation. The material properties of the FE models are considered as linear elastic without considering geometric nonlinearity.

The input material data are identified through an inverse method. Indeed, there are some adjustments to be done compared to the values given by the manufacturer due to the real state of the matrix and the test configuration. For that, an unrepaired specimen is extracted from a non-repaired zone of the 16 plies ±45° plates. These testing coupons, noted Ep 1, Ep 2 and Ep 3, are shaped in the form of a dumbbell (with wider end tabs and a narrow gauge area) in order to control the place where the testing coupon is expected to nucleate the first damage, (i.e. away from the clamps of the universal test machine). The beginning of the nonlinear part of the axial stress-strain curve (cf. Figure 16) serves to the inverse analysis leading to the elastic and limit values of shear strength and transverse strength matrix identifications (cf. Table 2 and Table 3).

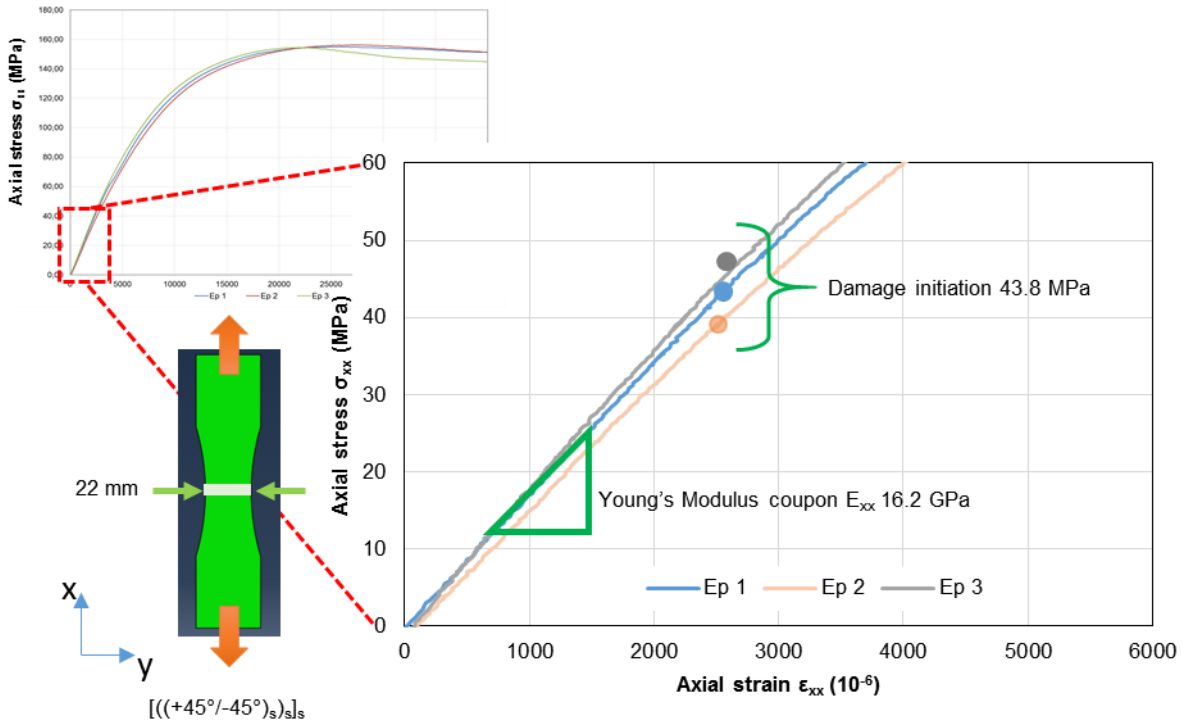

Figure 16. Inverse identification of the material properties (first damage initiation) using a tensile test on unrepaired specimens extracted from the mother plate.

The material properties of the Hexply® M21/35%/268/T700GC and the Hexbond® adhesive film are indicated in Table 2. The strength values used to calculate the Tsai-Hill (TH) criterion are indicated in Table 3. These values are entered into the FE model to compute the Tsai-Hill criterion for the composite material as a high probability of the occurrence of damage nucleation. As mentioned before, this test is mainly dominated by the shear and tensile matrix properties, and it is well below the maximum load capacity of the fibres (either in tension or in compression). The values for the tensile strength of the matrix (Y_T) and the shear strength (S) are below the typical epoxy values, as these values were identified to determine the damage initiation values on the ±45° test configuration. A Mixed Failure

criterion developed by [3] is used for the adhesive film. This criterion is based on the works of [5]. The input data are presented in Table 2.

Three different models are considered, one for each of the overlap lengths respectively, 6 mm, 8 mm and 13 mm.

Table 2. Material properties of the polymerised ply (in red the modified properties by inverse identification along reinforcement orientation) and the adhesive film.

UD Ply Hexply® M21/35%/268/T700GC		**Adhesive film Hexbond®**	
Property	***Value***	***Property***	***Value***
Axial Young's modulus E_1 (MPa)	140 500	Adhesive Young's modulus E_a (MPa)	3 800
Transverse Young's modulus E_2, E_3 (MPa)	10 100	Adhesive Poisson's ratio ν_a	0.300
Axial-transverse Poisson's ratio ν_{12}, ν_{13}	0.334	Mean adhesive thickness t_a (mm)	0.100
Transverse-transverse Poisson's ratio ν_{23}	0.171		
Axial-transverse shear modulus G_{12}, G_{13} (MPa)	4 600		
Transverse-transverse shear modulus G_{23} (MPa)	3 600		
Mean ply thickness t_{ply} (mm)	0.260		

Table 3. Strength of the polymerised ply (along reinforcement orientation, (in red the modified properties by inverse identification) of the UD Ply M21/35%/268/T700GC and the adhesive film.

Property	***Value***	***Property***	***Value***	***Property***	***Value***
Axial tensile strength X_T (MPa)	2 800	Transverse tensile strength Y_T (MPa)	20	Shear strength S (MPa)	23
Axial compressive strength X_C (MPa)	-1 700	Transverse compressive strength Y_C (MPa)	-300		
Average adhesive shear strength in the overlap (MPa)	35	Adhesive tensile strength (MPa)	70	Adhesive peel strength (MPa)	20

5. Results

Three coupons per overlap length were tested in a universal test machine. Here we illustrate with results concerning the 13 mm overlap repair length for the three specimens noted 13-1, 13-2 and 13-3. The non-repaired zone in the parent area was painted for digital image correlation in order to have the stress-strain curve of this particular area (cf. Figure 17). The zone, with the thinnest cross section because of 16 plies instead of 17 plies in the overlap and the reconstituted zone of the repair patch (cf. Figure 15), is the zone expected to have damage initiation before the others and especially before the adhesive joint repair patch.

The aim is to illustrate that the maximum loading flow (here the shear flow), when it is not applied in the reinforcement orientation, does not depend on the overlap length. This hypothesis is used to reduce the repair patch extension [2]. According to [2] along the fibre direction, the overlapping length depends on the chosen step ratio. In the other directions, this ratio can be reduced down to zero.

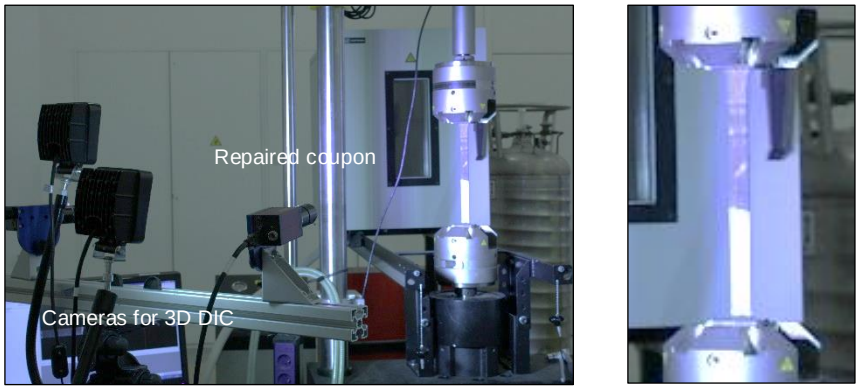

a) **b)**

Figure 17. Axial tensile test configuration with a) set-up with two cameras for 3D DIC and b) zoom of the repaired coupon with its DIC speckle (in white).

Comparing the test between the composite repaired specimens and the reference coupons, we cannot see any distinction in the mechanical behaviour (cf. Figure 18). At this moment of the test, the adhesive has not been damaged. Table 4 and Table 5 summarize the experimental results for the reference, non-repaired coupons, and the repaired coupons for the non-repaired parent area. We observe that the values for the Young's modulus, as well as the damage initiation limit are within the same order of magnitude.

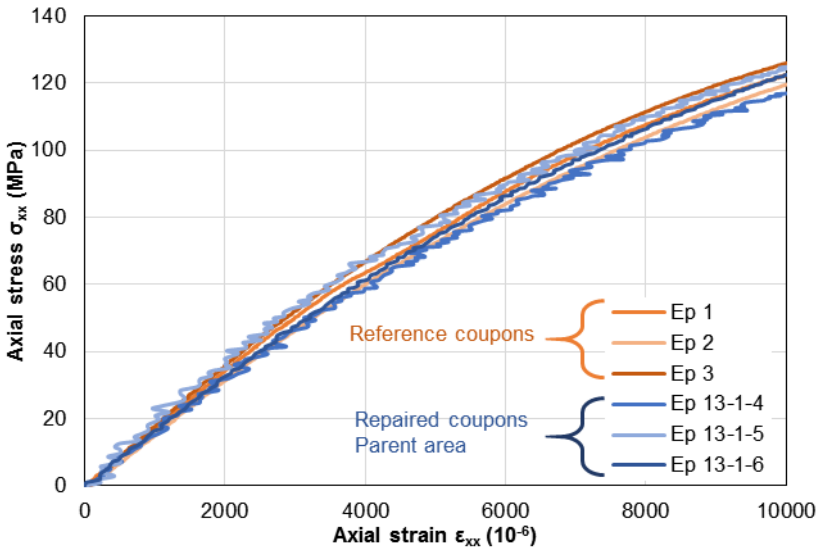

Figure 18. Axial stress σ_{xx} – strain ε_{xx} curve of the parent area of the repair coupons 13-1, 13-2 and 13-3 and the reference test coupons Ep 1, 2 and 3.

Table 4. Results of the reference test coupons Ep 1, 2 and 3

Properties	*Coupon*			*Mean*	*Std. deviation*
	Ep 1	**Ep 2**	**Ep 3**		
Axial Young's modulus E_{xx} (GPa)	16.3	15.5	16.9	16.2	0.70
Axial strain ε_{xx} (1E-6)	2 765	2 536	2 760	2 687	131
Axial stress σ_{xx} (MPa)	45.0	39.4	46.9	43.8	3.88
Load L (kN)	4.18	3.67	4.46	4.10	0.40

Table 5. Results of the reference test coupons Ep 13-1, 13-2 and 13-3.

Properties	*Coupon*			*Mean*	*Std. deviation*
	Ep 13-1	**Ep 13-2**	**Ep 13-3**		
Axial Young's modulus E_{xx} (GPa)	15.5	17.0	16.0	16.2	0.77
Axial strain ε_{xx} (1E-6)	2 625	2 844	2 823	2748	130
Axial stress σ_{xx} (MPa)	40.5	48.5	44.7	44.6	4.00
Load L (kN)	3.56	4.28	3.94	3.93	0.36

As expected, the place where the damage initiation is expected is at the parent zone (with cross section reduction) between the end tab and the overlap areas. It corresponds to the same situation in the reference coupons. The three overlap ratios exhibit the same behaviour (cf. Figure 19).

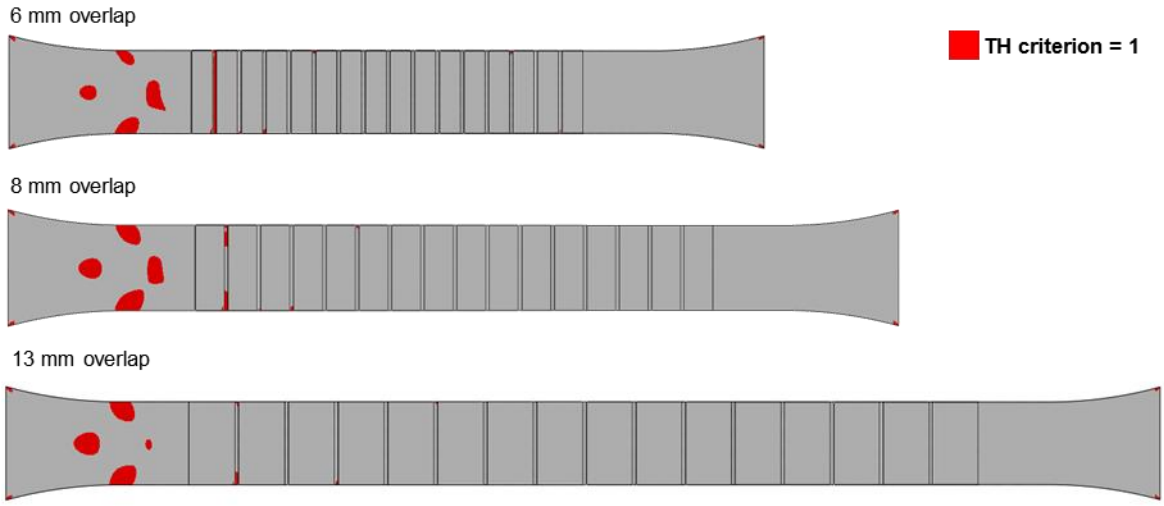

Figure 19. Tsai-Hill criterion (TH = 1 in red) in the FE models for the 6, 8 and 13 mm overlap lengths (from top to bottom).

As the adhesive elements are volume, they have information of the out of plane and transverse lap shear. Figure 20 shows the distribution of the shear stresses τ_{xz} at the bondline of each of the 16 steps for the three overlap ratios of 20, 30 and 50. We observe that the stress distribution is maximum at the extremities and minimum in the central steps but below the limit shear value (roughly 13 MPa), and, because of the test configuration, the peel stress values are negligible (less than 1 MPa which represents $1/20^{th}$ of the limit value, cf. Table 3). The stress values have the same order of magnitude for the three overlap ratios.

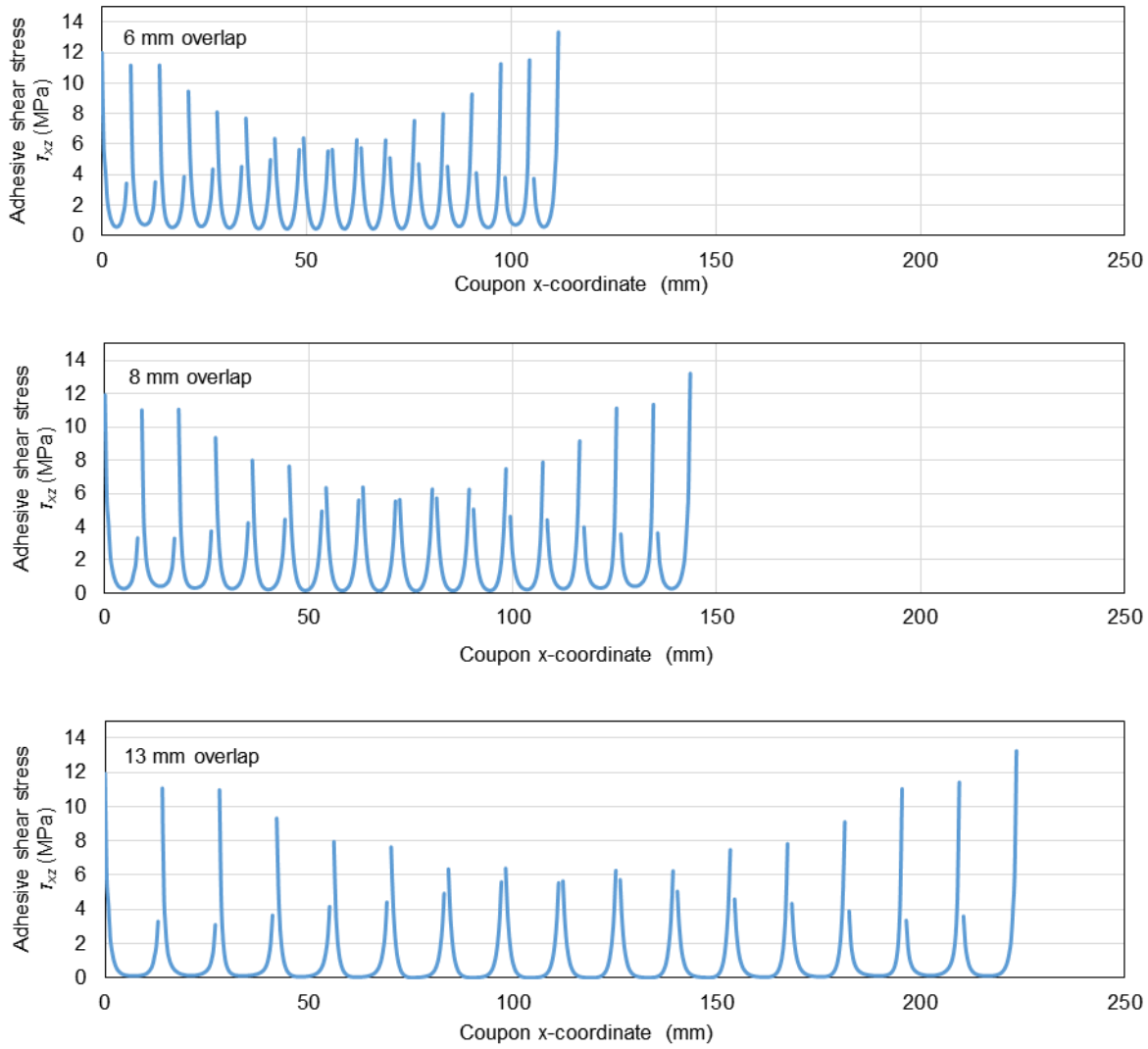

Figure 20. Shear stress τ_{xz} distribution in the adhesive in each step (from top to bottom) for the 6, 8 and 13 mm overlap lengths.

Since the distribution of shear stress is not uniform along the bondline, where there is a pike in stress at both ends of the overlap, while the stress values are very close to zero at the middle of the bondline. These results are in accordance with classical results in the literature [5]. For this reason, a criterion to determine whether the bond has failed by shear stress is to obtain the area under the curve, which is the total stress per unit length that the adhesive carries (cf. Figure 21). The average shear strength for the adhesive along the overlap is roughly 35 MPa.

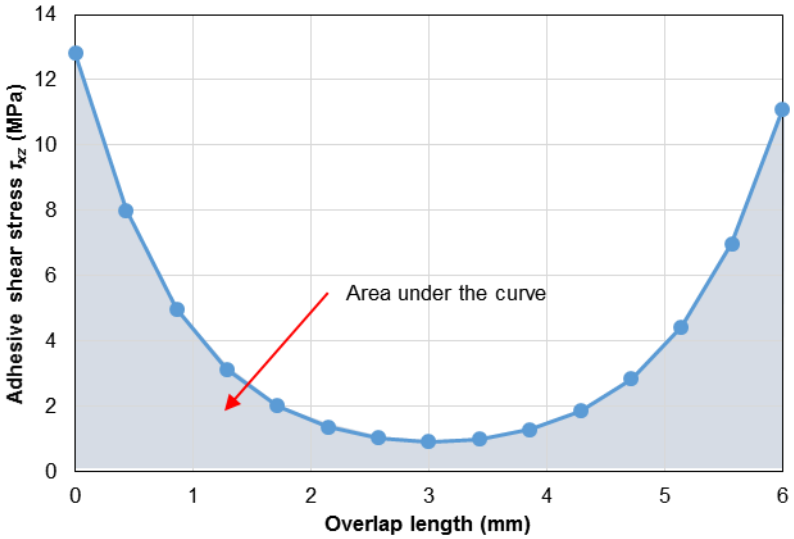

Figure 21. Illustration of the determination of the average shear value along the adhesive joint for 6 mm overlap length.

The FE results show that at a load corresponding to the damage initiation in the parent composite (TH = 1, cf. Figure 19), the maximum shear value calculated in the adhesive (area under the τ_{xz} curve) is 13.5 MPa in both step 1 and step16, and the rest of the steps in between having a less significant value (cf. Figure 22). All overlap lengths (6, 8 and 13 mm) exhibit the average shear lap stresses in the same order of magnitude.

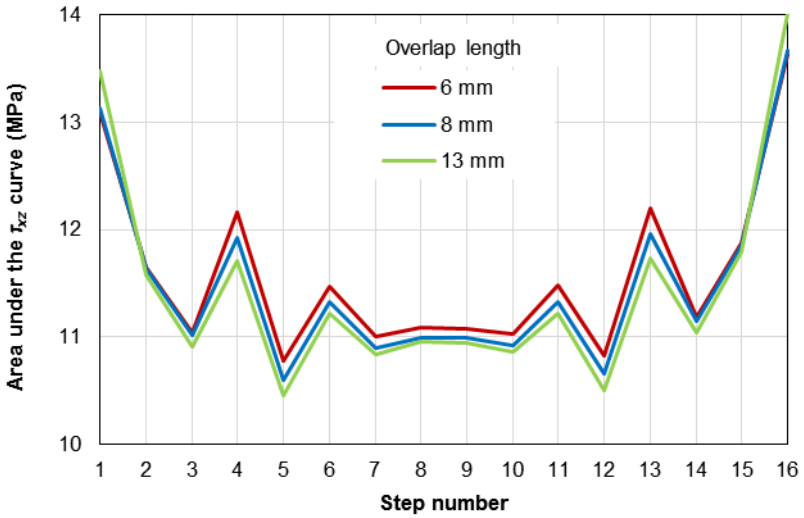

Figure 22. Area under de curve τ_{xz}-step length at each step and for the 6, 8 and 13 mm overlap lengths.

Finally, Table 6 summarizes the data obtained by the FE models highlighting that the three 20, 30 and 50 overlap ratios (corresponding to 6, 8 and 13 mm overlap lengths respectively) yield to the same orders of magnitude for the maximum axial strain ε_{xx} in the non-repaired parent area. This suggests an interest to the reduction of the overlapping length [2].

Table 6. Results of the FE models at the "saturation" of the Tsai-Hill criterion (TH=1 for damage matrix initiation)

Overlap length (mm)	6	8	13
Load L (N)	3 980	3 980	3 980
Displacement u_x of the mobile clamp (mm)	0.52	0.60	0.80
Max area under the curve of τ_{xz} (MPa)	13.63	13.66	14.01
Max axial strain ε_{xx} in the non-repaired parent area (10^{-6})	2 728	2 722	2 764

6. Conclusions

In this paper, the different stages of a repair process on an aeronautical composite material have been presented.

First, the machining tool generates an abrasive waterjet with specific parameters adapted to composite blind machining [6]. A control system captures and analyses images to generate a mapping of the machining work both between each machining step to adapt the depths to the ply thickness variability [7], and to archive the result when the repair machining work is complete.

Secondly, the repair procedure is followed using the industrial set-up a hot bonder. The studied plate of 16 plies of UD Hexply® M21/35%/268/T700GC prepreg with a stacking sequence $[+45/-45/-45/+45/+45/-45/-45/+45]_s$ is repaired for 3 overlapping lengths (6, 8 and 13 mm) according to the aeronautical requirements.

Third, for the different overlapping lengths, a cross-over of computational tests with specimens taken from the repaired motherboard and subjected to an axial effort. The mechanical tests exhibit that the repaired zones are not the weak link of the specimens whatever the overlap lengths.

Fourth, an innovative multi-scale model is used in which only the adhesive zone consists of volume finite elements. The FE results show that at a load corresponding to the damage initiation in the parent composite, the maximum shear value calculated in the adhesive is reached under the maximum shear whatever the steps and the overlap lengths.

This illustrates that the joint patent [2] held by the Clement Ader Institute, the SME Composites Expertise & Solutions and the TPE Bayab Industries operates because it is based on the simple idea that a nominal overlapping length is only necessary if strictly in the direction of the UD ply fibres. It is shown that this approach makes it possible to reduce the grip of repair patches by more than 70 % [4], making the adhesive patch certifiable by aeronautical certification authorities. To be close to an industrial application, an original methodology of mechanical characterization (called Multi-Instrumented Technological Evaluator tool box [4]) has been proposed. The MITE tool box allows the design of a case specific repair evaluator that can be tested in a multi-axial testing machine under complex loading sequence. Finally a French repair workshop exists since 2010 in the GDR 3371 MIC (Composite Manufacturing and Induced Properties), showing the relevance of the French composite repair activity, in particular at Clement Ader Institute in cooperation with the SME Composites Expertise & Solutions.

References

[1] Hanser, S., Ferrer, G., Dupouy, S. A350 XWB composite bonded repair, New technology for new aircraft, pp 11-18, Fast#61, 2018.

[2] ca 2769668**,** Method for repairing a wall consisting of a plurality of layers, filling date: 28-07-2010, publication date: 17-02-2011. Owners: Jedo Technologies then Bayab Industries (France), Composites Expertise & Solutions (C.E.S.) (France), Institut Clément Ader - Université Paul Sabatier (France), http://bases-brevets.inpi.fr/en/document-en/FR2949092.htm, 2010.

[3] Cerisier, A. Prediction of the behavior of a primary step-lap bonded repair : application of a methodology with technical evaluators, Ecole doctorale MEGeP, Institut Clément Ader (ICA-Toulouse), Toulouse III PhD thesis (in French), 2017.

[4] Collombet, F., Grunevald, Y.H., Crouzeix, L., Douchin, B., Zitoune, R., Davila, Y., Cerisier, A., Thevenin, R. Chapter 10 Repairing composites, in book Advances in Composites Manufacturing and Process Design, Chap. 10, Elsevier Ltd. ISBN: 978-1-78242-307-2, pp. 197-227, 2015.

[5] Cognard, J.Y., Sohier, L. and Davies P. A Modified Arcan Test to Analyze the Behavior of Composites and Their Assemblies Under Out-of-plane Loadings. Composites Part A: Applied Science and Manufacturing 42.1, pp. 111–121, 2011.

[6] Cénac, F., Collombet, F., Déléris, M, Zitoune, R. Chapter 4. Abrasive Water Jet Machining of Composites, p.167-180, Machining Composite Materials, Paulo Davim, J., ed., ISTE Ltd, 2010.

[7] Davila, Y., Crouzeix, L., Douchin, B., Collombet F., Grunevald Y-H. Spatial Evolution of the Thickness Variations over a CFRP Laminated Structure. Applied Composite Materials, 24(5), pp. 1201 - 1215, 2017.

Acknowledgments

The authors acknowledge CONACyT of Mexico for the PhD scholarships provided to Sergio Albano Avila Hernandez and, Alexander Morales Gomez. The authors want to declare their gratitude for his helpful advice to Sebastien Dupouy, A350 Industrial Manager of Aircraft Repairs & Retrofits, and Guillaume Ferrer, Embodiment Industrialization Manager, in charge of A350 composite repair process development and the Repair LAB in Airbus Customer Services. We would like to thank Olivier Cherrier and Marc Chartrou from Clément Ader Institute for their valuable contribution to the mechanical tests and Thomas Beaucourt, technician in Bayab Industries for the machining of the composite plates.